Brazilian Journal
of Chemical
Engineering

ISSN 0104-6632
Printed in Brazil
www.abeq.org.br/bjche

Vol. 36, No. 03, pp. 1143 - 1154, July - September, 2019
dx.doi.org/10.1590/0104-6632.20190363s20180415

AN INVESTIGATION OF THE HEAT TRANSFER PERFORMANCE OF DUAL IMPROVED INTERMIG IMPELLERS IN A STIRRED TANK WITH AN INNER HEATING COIL

Yongjun Zhou[1]*, Leizhi Wang[1] and Binwei Jiang[2]

[1] Nanjing Tech University, School of Mechanical and Power Engineering, Nanjing, China.
E-mail: zhouyj@njtech.edu.cn
[2] China National Offshore Oil Corporation Petrochemical Engineering Co., Ltd., China. ORCID: 0000-0002-7046-245X

(Submitted: August 30, 2018 ; Revised: April 12, 2019 ; Accepted: April 12, 2019)

Abstract - The heat transfer process in a stirred tank of diameter T=0.5m equipped with dual-layer improved Intermig impellers and helical coils was investigated by experiment and numerical simulation methods. The temperature field, the temperature boundary layer lateral to the coil and the heat transfer coefficient were measured at different rotational speeds. The standard k-ε turbulence model and multiple reference frames combined with a sliding mesh method were adopted in the numerical simulation. The results show that the temperature errors between numerical simulation and experimental measurement were within 2K. The temperature in the stirred tank gradually rose from top to bottom and inside to outside, and the maximum temperature difference was within 2K. The average thickness of the temperature boundary layer outside the helical coil is 3.66 mm. According to the experiments and numerical simulations, the heat transfer coefficient correlations, including Nu and Re, Nu and ε of the helical coil outer side, were obtained, and the trends of heat transfer coefficients are consistent and regular. The correlation of the heat transfer coefficient lateral to the coil was acquired from the experimentally measured data. The research results can serve as a guide for the design and engineering application of mass and heat transfer processes in stirred tanks with improved Intermig impellers.
Keywords: Improved intermig impeller; Temperature field; Temperature boundary; Heat transfer coefficient correlation.

INTRODUCTION

The Intermig impellers are an improved version of the MIG impellers, which were developed by the German company EKATO. When the Intermig impeller was introduced in China to replace the traditional axial flow paddle in the aluminum industrial seed tank , the stirring effect had a significant improvement, and it became the improved Intermig impeller after repeated modifications (Zhao et al., 2014). The photographic views of MIG, Intermig and improved Intermig impeller are shown in Fig 1(a), (b), (c). The model of MIG contains two opposite angle impellers in Fig 1(a); the Intermig impeller structure changed by doubling the end part of MIG blade. Houcine et al. (2000) studied the power consumption and stirring efficiency of double-layered Intermig blades in Fig 1(b) compared to other conventional blades through experimental research. They drew a significant conclusion that the Intermig impeller possesses not only better mixing effect, but also lower power consumption among that impellers. Ibrahim et al. (2004) studied the solid-liquid suspension characteristics of Intermig impellers and two other axial flow paddles and found that Intermig greatly improved the results of suspension dispersion rate. An improved Intermig impeller model is shown in Figure 1(c). Its main feature is that the separation angle between the axis and the inner blade is 60 °, and

* Corresponding author: Yongjun Zhou - E-mail: zhouyj@njtech.edu.cn

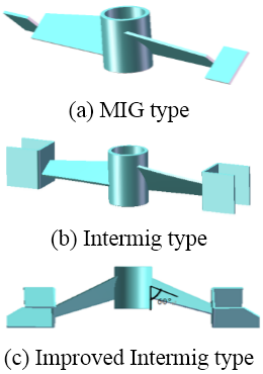

Figure 1. Related impellers during the evolution of the improved Intermig impeller.

the sub-blade bottom on the front side of the agitation direction is lengthened. This is similar to the upper pumping inclined blade of a turbine (Wang, Cunteng et al, 2018), and the improved impeller can provide an intense axial flow effect.

Concerning related flow field researches, Szalai (2004) examined that the computed velocity field and mixing patterns under Reynolds numbers 37, 50, and 100 using PIV, acid-base visualization experiment and Planar Laser-Induced Fluorescence methods. The conclusion was that a separation plane exists in the tank at mid-height, which forms a vital barrier to mixing in the axial direction. The solution of the problem is to vary the rotational speed at periodic intervals of time to break the vertical separation plane. Hidalgo-Millán et al. (2012) compared the mixing performance of the straight Maxblend with a double stage pitched blade turbine (PBT) and double Ekato Intermig impellers under same specific power. The results of the flow fields show that the straight Maxblend behaves much better in terms of the fluid circulation in the vertical direction.

In addition-related studies for the improved Intermig impeller have been performed on solid-liquid suspension and power consumption (Xie et al., 2014; Zhao et al., 2015). It is noteworthy that the above studies did not involve the heat transfer performance of the Intermig impeller or improved Intermig impeller in a stirred tank. In actual industrial production, stirred reactors are generally accompanied by a heat transfer process. During the heat transfer process, an internal helical coil is sometimes required to increase the heat exchange surface area in the stirred tank. Therefore, it is extremely important to study the heat transfer process of the improved Intermig impeller in stirred tanks with inner heating coils. However, studies of the heat transfer inside a stirred tank with an improved Intermig impeller has rarely been reported.

Many research reports have been published on heat transfer in stirred tanks with other types of impellers. Delaplace et al. (2001) utilized experimental and simulation methods to study the heat transfer of highly viscous fluids in an agitated vessel equipped with a non-standard helical ribbon impeller, and numerical simulations of heat transfer phenomena in a highly viscous Newtonian fluid in unsteady states in a jacketed vessel were attempted using CFD finite element software. In order to monitor the thermal boundary layer thickness and its renewal with the impeller rotation (Delaplace et al., 2005), heat flux sensors were used to replace the conventional thermocouples to determine the instantaneous heat transfer coefficients of a jacketed stirred tank with non-standard impellers. Lubomira et al. (2008) studied the boundary layer friction coefficient and heat transfer coefficient distribution in non-Newtonian fluid stirred tank equipped with six different agitators such as turbine and paddle and demonstrated that, for determination of the flow and heat transfer characteristics in agitated non-Newtonian media, the electrochemical method can be very useful. Triveni et al. (2008) studied the effects of parameters such as diameter and speed of anchor and turbine agitators on the heat transfer coefficient in stirred tanks of Newtonian and non-Newtonian fluids with inner coil heating. With reasonable power consumption, large heat transfer coefficients are realized when scaleup is based on equal power per unit volume as scale up criteria. The reliable relationships based on the dimensional analysis of conservation equations of mass, momentum and energy are obtained by model geometrical parameters such as the following equations (1) and (2).

$$Nu = C\,Re\left[\left(\frac{1+2a}{n+1}\right)+b\right]Pr^{c}\,Vi^{d}Fr^{e}B^{(f(n-1))}\left(\frac{(3n+1)}{4n}\right)^{gn} \quad (1)$$

$$Nu = C\,Re\left[\left(\frac{1+2a}{n+1}\right)+b\right]Pr^{c}\,Vi^{d}Fr^{e}K_{s}^{f(n-1)} \quad (2)$$

Kanamori et al. (2011) developed a new method for measuring the heat transfer coefficient at the inside wall of an agitated vessel in the high Reynolds number region, and this method was used to test the effect of the speed, the baffle conditions, and distance between the paddle and the vessel bottom on the heat transfer coefficient in the stirred tank with four kinds of blades such as turbine and paddle. With decreasing distance from the bottom, the heat transfer coefficient *h* increased gradually under various rotational speeds. And the influence of the flow pattern and flow velocity on the *h* distribution in a stirred tank was made clear. Liu et al. (2013) utilized experimental and simulation methods to study the heat transfer performance of a new type of combined coaxial agitator in a jacketed heating stirred tank. The results show that the heat transfer coefficient near the inner wall of the tank increased when the speed of the inner paddle or

outer paddle increased, but the speed of outer paddle hardly affected the heat transfer coefficient. What is more, the heat transfer performance of double-shaft mixing is much better than that of single-shaft mixing. In addition, Dostál et al. (2014) adopted the transient method based on measuring the temperature dependency on time and solving the unsteady enthalpy balance to determine the heat transfer coefficient between the agitated liquid and the helical pipe coil. Delgado et al. (2017) conducted experimental studies on the heat transfer process in a stirred tank with internal heating coils using a phase change material (PCM) emulsion as a thermal energy storage system and determined the heat transfer coefficient between the spiral internal heating coils and the PCM emulsion.

The above literature is more concerned with the new heat transfer research method in the stirred tank and the agitators involved are mostly conventional blades such as turbines, anchors and paddles. Furthermore, most researchers found that, under various working modes, such as speed or distance between the impeller and the vessel bottom, heat transfer coefficients are influenced by geometrical model parameters. Systematic conclusions on the improved Intermig impellers have been little drawn in terms of agitation heat transfer, but the application of engineering lacks beneficial information for the stirred tank with the improved Intermig impellers. In this paper, three methods are used to investigate heat transfer efficiency: a testing temperature experiment with new type touching thermocouples, a simulation method and comparison with empirical fitting formulas, which identified reliable results of the heat transfer model. Meanwhile, fitting equations for the heat transfer model of the improved Intermig impellers are obtained in order to design a novel mixing device. Lastly, torque and power consumption are not completely considered in these papers. The energy consumption of a stirred system should necessarily be optimized because this is an important parameter limiting the heat transfer enhancement in the stirred tank. Under different rotational speeds the power is tested by experiment and by simulation. The relationship between the heat transfer coefficient of the outer wall of the coil and unit volume work is investigated comprehensively compared with previous works. The research results can serve as a guide for the design and engineering application of mass and heat transfer processes in stirred tanks with improved Intermig impellers.

EXPERIMENTAL SECTION

Experimental Measuring Equipment

Based on the console especially developed for testing the impeller performance, the speed of the impeller is controlled by connecting the Siemens MM420 converter in the platform with a computer. The lifting platform is powered by a hydraulic device in order to adjust the installation position of the double impeller and the impeller pitch. Most importantly, the heating unit employs a steam generator on the left side of the stirred tank with an evaporation capacity of 120 kg/h. Steam of high temperature produced by a steam generator, flows into coil pipes and heats the stirred fluid by the pipe wall. The temperature of the helical coil outside wall is measured with 6 thermocouples, and the body temperature in the stirred tank is measured with 9 armored thermocouples. In addition to the measurement of temperature, the performance parameters such as power of agitator and mixing efficiency can also be tested through the platform. The torque meter is installed on top of the shaft and connected to the secondary instrument displaying data of torque values. The platform for the experiments is shown in Figure 2. The control and measurement of the speed, temperatures, torque, and platform lift are all centralized in the control cabinet.

The experiment utilized a stainless-steel stirred tank with a standard ellipsoidal bottom. The tank's inner diameter is D_0, and its height is H. The inner heating coil has a centre diameter D_1, wire diameter Φ, and thread pitch S. C_1 is the distance from the lower impellers to the tank's bottom, and C_2 is the distance between the two layers of impellers. A full-baffle configuration is used, and the baffle width is W_B. The working fluid is water, and the height of the liquid is h. The dual-layer improved Intermig impellers are arranged orthogonally. The impeller diameter is d, and the inner and outer impeller angles are 45 degrees and -45 degrees, respectively. The inner impeller is inclined 30 degrees downward in the direction of the impeller shaft. The tank body and impeller structure are shown in Fig 3, and the dimensions are listed in Table 1.

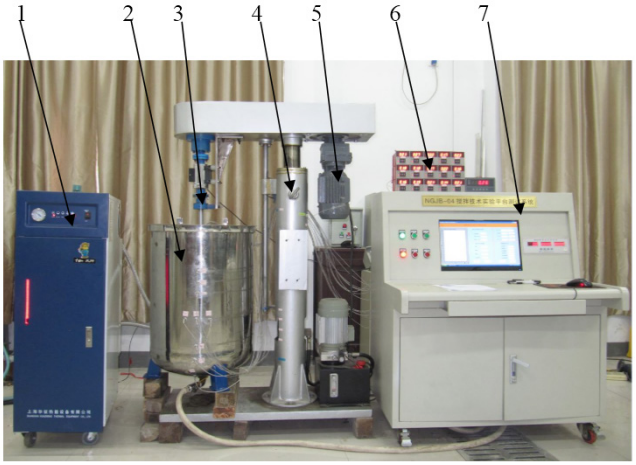

1. Steam generator 2. Stirred tank 3. Torque meter 4. Hydraulic lift device 5. Speed drive unit 6. Temperature control instrument 7. Control cabinet.

Figure 2. Platform for the experiments.

Table 1. Basic structural parameters of the stirring system.

Parameters	d	D_0	H	D_1	Φ	S	W_B	h
Dimensions(m)	0.21	0.5	0.75	0.33	0.02×0.002	0.05	0.04	0.6

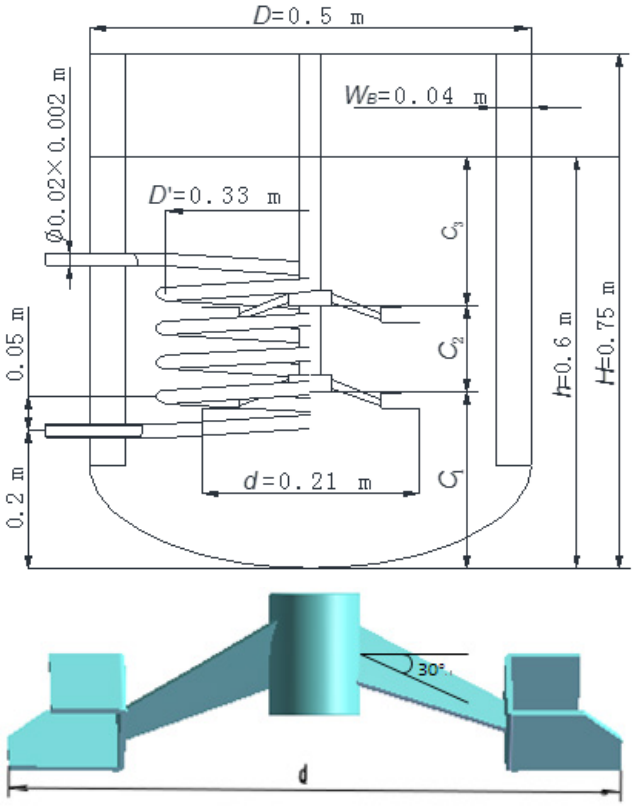

Figure 3. Schematic diagrams of the stirred tank and the improved Intermig impellers.

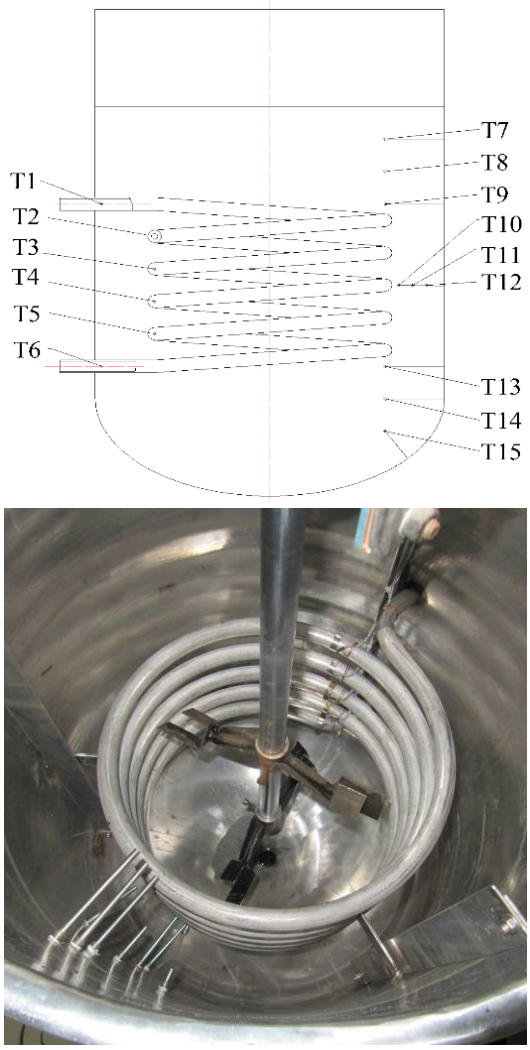

Figure 4. Layout of the temperature measurement points.

Parameter Measurement

T1/T2/T3/T4/T5/T6 are the temperature measurement points of the helical coil. The thermocouples are connected to a metal ring by the isotherm contact method, and the metal ring is fixed tightly to the coil with a screw. The body average temperature in the tank is measured by armoured thermocouples T7-T15 with a diameter *Φ* of 6 mm. The temperature measurement points are arranged outwards from the heating coil in a star shape. The detailed layout of the temperature measurement points is shown in Fig 4.

At a unit pressure-volume power *ε*, the power in the improved Intermig impellers must be measured at different speeds. During the experiments, the stirrer shaft torque is measured by the torque meter that is connected to the end of the stirrer shaft. The measured stirring powers are then calculated, and they are tabulated with the corresponding simulation values in Table 2. The powers measured in the experiments are greater than the simulated results. The variation between the experiments and simulations decreases with increasing rotation speed. With the increasing growth of difference between measured and simulated power, it can be seen that the maximum difference is 1.273 W at 180 r/min and the minimum difference is 0.046 W at 40 r/min. The results show that there may be a large power error between experiment and simulation when the rotational speed become higher than before. On the basis of measuring power at different speeds, the improved Intermig impellers could suffer pressure and viscous forces in the fluid field, resulting in the moment acting on the stirrer shaft, which is sum of M1 generated by the pressure gradient and M2 of the shear stress generated by the viscous force, as shown in Equation (3).

$$M = M_1 + M_2 \tag{3}$$

Stirring power is shown in Equation (4), where M is the torque (N . m) and ω is the stirring impeller angular velocity (r/s)

Table 2. Experimental and simulated powers at different rotational speeds.

Rotational speed (r/min)	40	60	90	120	150	180
Measured torque (N·m)	0.06	0.11	0.17	0.30	0.46	0.65
Simulated torque (N·m)	0.049	0.095	0.146	0.259	0.405	0.582
Measured power (W)	0.251	0.692	1.602	3.770	7.226	12.252
Simulated power (W)	0.205	0.597	1.376	3.257	6.357	10.979

$$P = M\omega = \left(M_1 + M_2\right)\omega \tag{4}$$

Principle of the heat transfer process

The fluid in the stirred tank is heated by water vapor in the inner coil and the heat transfer process can be described as follows (Perarasu et al., 2012):

$$Q = K_o A_o \Delta T_{ln} \tag{5}$$

$$A_o = \pi d_o l \tag{6}$$

$$\Delta T_{ln} = \frac{\left(T_B - T_i\right) - \left(T_B - T_o\right)}{\ln \dfrac{\left(T_B - T_i\right)}{\left(T_B - T_o\right)}} \tag{7}$$

A_o is the helical coil surface of heat transfer in formula (6) andΔT_{ln} is the logarithmic mean temperature that was used for calculating the actual overall rate of heat transfer Q.

$$Q = Q_c + Q_s = \Delta E_m + \Delta E_w + Q_h \tag{8}$$

$$Q_c = M\left(C_p\right)_{cw}\left(T_o - T_i\right) \tag{9}$$

The actual overall rate of heat transfer Q originates from the steam generator and the work done by the mechanical stirring. For a low viscosity fluid, the effect of the work Q_s by mechanical stirring is not significant and is generally negligible. Thus, the actual overall rate of heat transfer Q is approximately equal to the heat flow Q_c generated by the high-temperature steam. The main forms of energy dissipation include the increase in entropy ΔE_m of the main body material, the increase in internal energy ΔE_w due to the increased reactor wall temperature, and convective heat dissipation Q_h from the reactor body to the air. The reactor wall mass and the specific heat capacity of the metallic material are significantly less than those of the main body material, and the heat dissipation from the reactor wall surface to the air is very limited.

$$K_o = \frac{Q}{A_o \Delta T_{ln}} \tag{10}$$

$$\frac{1}{K} = \frac{1}{h}\frac{d_o}{d_i} + \left(\frac{x_w}{k_h}\right)\left(\frac{d_o}{d_o - d_i}\right)\ln\frac{d_o}{d_i} + \frac{1}{h_o} \tag{11}$$

In formula (11), h_o is the convection heat transfer coefficient of the outside surface of the helical coils; h_i is the convection heat transfer coefficient of the inside surface of the helical coils; k_h is the thermal conductivity of the helical coils.

$$Nu = 0.042\,Re^{0.629}\,Pr^{1/3}\left(\frac{\mu_{cw}}{\mu_w}\right) \tag{12}$$

As the heating fluid mass flow is fixed at 0.0333kg/s and the Reynolds number for this flow rate based on the inside diameter of the heating coil is around 8000, the empirical equation (12) is used for calculating the inside coil heat transfer coefficient (Dostál et al., 2014).

In formula (13), h_i is the convection heat transfer coefficient of the inside surface of the helical coils. Knowing K_o and h_i, the outside heat transfer coefficient h_o was calculated using the relation (14). The Nusselt number for the outside heat transfer coefficient in a stirred tank with dual improved Intermig impellers was calculated as in Eq. (15). This method of calculation using the heat transfer coefficient h_i of the inside coil wall deduces the heat transfer coefficient h_o of the outside coil wall in formula (14), and the Nusselt number in formula (15) is then obtained from h_o, d_o and k_o.

$$h_i = \frac{Nuk_i}{d_i} \tag{13}$$

$$h_o = \frac{1}{\left\{\dfrac{1}{K_o} - \left[\dfrac{1}{h_i}\dfrac{d_o}{d_i} + \left(\dfrac{x_w}{k_h}\right)\left(\dfrac{d_o}{d_o - d_i}\right)\ln\dfrac{d_o}{d_i}\right]\right\}} \tag{14}$$

$$Nu = \frac{h_o d_o}{k_o} \tag{15}$$

During the indirect operation of a constant temperature heat carrier, the process is heating the working medium from room temperature 25°C to a temperature T_o within the time θ. For the experimental study of the convective heat-transfer coefficient outside the coils, the coil wall temperature and the total temperature change per unit time must be monitored. The coil wall temperature is calculated, and the average coil wall temperature collected during the

entire process is used as the qualitative temperature. The experimentally measured temperatures at the monitoring points increase linearly over a short period of time. The energy dissipation from stirring and the impact of the surfaces on the measuring points lead to several temperature fluctuations during the initial stage, and the temperature at each point then stabilizes.

NUMERICAL SIMULATION

Numerical grid model

The simulation model is consistent with the experimental configuration. Due to the complicated structure of the improved Intermig impellers and the inner heating coils in the stirred tank, the turbulence in the target area is relatively intense, and the fluid exchange between the dynamic and static areas is relatively large. Furthermore, because some of the contents require a non-steady-state simulation, this paper uses a combination of the multiple reference frames method and the sliding mesh method for the simulations. The pre-processing software Gambit, which is recommended by Fluent, is used to build the models. To improve the quality of the mesh, the baffle is simplified, and many of the coil ends that overlap with the baffle are also simplified.

The geometries and meshes model are created using the software ANSYS, version 17.0. Considering the accuracy of this model, the whole reactor is modelled as the system investigates rotational periodicity of heat transfer. (Prada and Nunhez, 2017) The area inside the stirred tank is divided, and an unstructured mesh is used to further divide the tank. To improve the mesh quality in the impeller area, the meshes for the impellers and the stirring shaft are refined in advance by the software Gambit. The surface meshes of the impeller surfaces and the outside coil wall can be generated first and the meshes in the vicinity of the impellers and coil are created by the principle of topology of numerical grids using the block tool in Gambit. Because the temperature gradient at the inner heating coil is large, the boundary layer mesh processing is performed based on the refined meshes of its surface. The detailed model and the mesh structures are shown in Figure 5. A total of approximately 1.2 million mesh cells are used. This mesh contains 1.2×10^5 elements in the rotating domain and 1.08×10^6 elements in the stationary domain. Additionally, 8 elements inside the boundary layer of the coil are taken into account to ensure excellent results for the heat transfer model. The mesh was verified to meet the accuracy requirements.

The Physical Properties of the simulation

Water was used as fluid in the simulation, and it was assumed to be incompressible. Because the temperature of the water inside the stirred tank does not change significantly during the experiments, the physical properties are assumed to remain constant during the calculations. The physical properties of water at an average temperature of 323 K are used, including the density ρ=988.1 kg/m^3, kinematic viscosity $v=5.56\times10^{-7}$ m^2/s, dynamic viscosity $\eta=5.494\times10^{-4}$Pa·S, thermal conductivity λ=0.6478 W/(m·K), heat capacity C_p=4.174 kJ/(kg·K), and Prandtl number $Pr=(\mu C_p)/\lambda$=3.45.

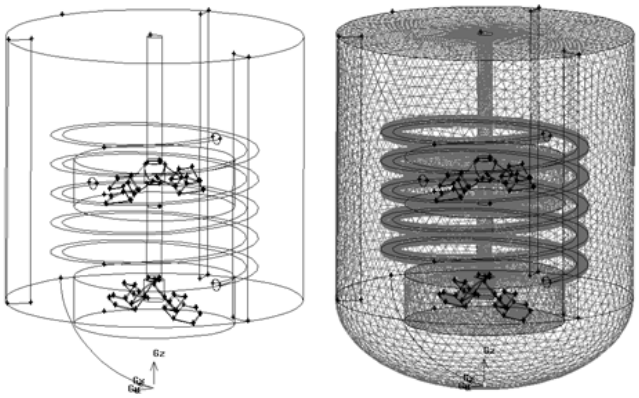

Figure 5. Calculation model and mesh.

Control equations of Numerical Simulation

The actual flow in the agitator is unsteady, but the variation of the flow with the impeller rotation is not very obvious. Considering the long calculation time required for the simulation using the unsteady slide mesh model, it is not necessary to carry out the unsteady study. Multiple reference frames are used to process the flow in the agitator. It is considered that the flow in the agitator is constant flow, and the temperature field does not change with the relative position of the impeller. The simulation uses the steady-state method, in which a constant temperature less than the coil temperature is given for the wall based on the non-steady state simulation settings. Thus, a stable temperature field is obtained. The heat transfer parameters are acquired using the built-in post-processing program in Fluent. The standard k-ε turbulence model is used in the simulation (Zakrzewska and Jaworski, 2004; Kougoulos, 2005). A combination of the multiple reference frames method and the sliding mesh method is used to process the mixing model (Liu et al., 2013). First, with the energy equation turned off, the multiple reference frames method and steady state model are used to calculate the stable fluid field inside the stirred tank as the initial value. The energy equation is then turned on, and the instantaneous sliding mesh model and non-steady state method are used to perform the calculations of the heating processes. For the absolute speed formula, the steady-state fluid flow can be expressed by the following formula (Perarasu et al., 2013):

$$\frac{\partial \rho}{\partial t} + \nabla \rho v_r = 0 \quad (16)$$

$$\frac{\partial}{\partial t}\rho v + \nabla\left[\rho v_r v + \rho\left(w + v\right)\right] = -\nabla p + \nabla \tau + F \quad (17)$$

$$\frac{\partial}{\partial t}\rho E + \nabla\left[\rho v_r H + p u_r\right] = \nabla\left(K\nabla T + \tau v\right) + S_h \quad (18)$$

Eq. (16) is conservation of mass, Eq. (17) is conservation of momentum and Eq. (18) is conservation of energy. These basic governing equations and the governing equations of fluid flow for a steadily rotating frame were solved using the segregated solver.

The flow flied of the Intermig impellers in the agitator can simplify a certain position of the flow field, so constant methods are used to solve unsteady problems. The numerical grids of the stirred stationary zone are not moved when the model is calculated. The Coriolis force and centrifugal force are used to calculate in inertial coordinate system. The fluid parameters are exchanged to keep the continuity of the interface located between the moving and stationary zones.

$$\frac{\partial \vec{v_r}}{\partial t} + \vec{v_r} g \nabla \vec{v_r} + 2\vec{\Omega} \times \vec{v_r} + \vec{\Omega} \times \vec{\Omega} \times \vec{r} + \frac{\partial \vec{\Omega}}{\partial t} \times \vec{r} = -\frac{1}{\rho}\nabla \tau + \vec{f} \quad (19)$$

The term $2\vec{\Omega} \times \vec{v_r}$ on the left side of equation (19) is the Coriolis acceleration and $\vec{\Omega} \times \vec{\Omega} \times \vec{r}$ is the centrifugal acceleration.

RESULTS AND DISCUSSIONS

Reliability of the Models and Experiments

Using the rotating speed N=90 r/min in the stirring vessel as an example, the results of the numerical simulations and the measured changes in temperature are shown in Figure 6. At the same initial temperature, the average temperature changes linearly over a short period of time, during which the temperature is experimentally measured. The numerical simulation is close to the temperature measured by the experiment and the maximum error between the numerical simulation and experiment is less than 2 K.

The trends of the numerically simulated and experimentally measured temperature changes at other rotational speeds are similar, which indicates that the finite element model is accurate and that the experiments and simulations meet the requirements for studying the heat transfer process of the dual-layer improved Intermig impellers.

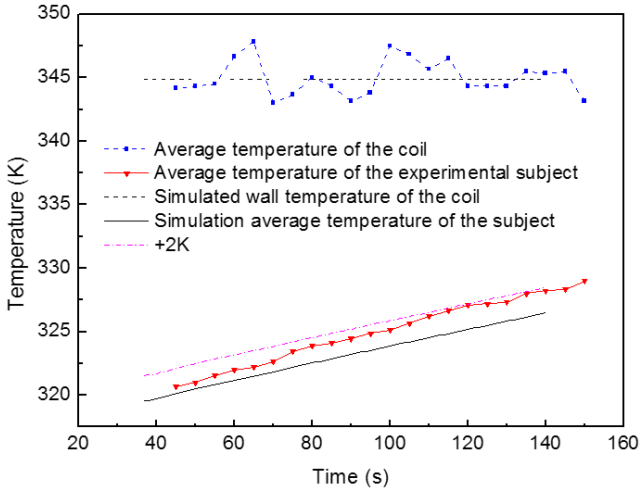

Figure 6. Comparison of the temperature changes in the numerical simulations and experiments at *N*=90 r/min.

Temperature field of the heat transfer process

The left part of Figure 7a shows the temperature field at 90 s with a rotational speed N of 90 r/min. The image of the temperature field clearly shows the isotherm distribution, and the heating temperature around the coil wall between the upper and lower impellers is relatively clear. The right part of Figure 7a shows the fluid flow field under these conditions, which clearly shows that the upper helical coil is washed by the fluid jetted by the upper impellers. Figure 7b shows the distribution of horizontal planes at four heights (a, b, c, d), in which a is at the level of the coil outlet, b is at the level of the upper impeller, c is halfway between the two impellers, and d is at the level of the lower impeller.

After stirring for 90 s, the average main body temperature of the medium has increased by 2 K. There is no obvious high temperature region, and the temperature boundary layer is thin. However, the intense heat exchange induced by the turbulence affects the shaft's power consumption, and the high shear flow must be controlled in certain reactions. The

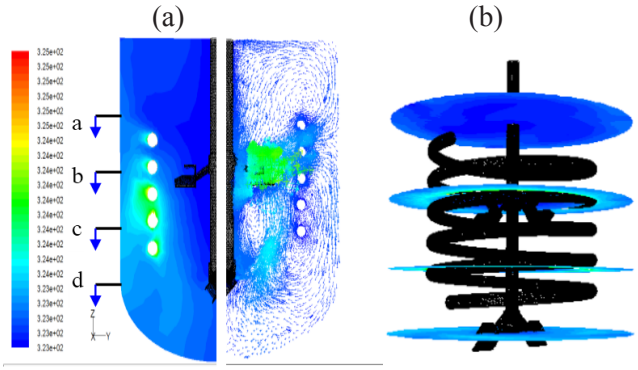

Figure 7. Longitudinal sections of the temperature field and velocity field (a) and the horizontal sections (b).

temperature in the reactor increases from the top to the bottom and from the inside to the outside; however, the maximum temperature difference is less than 2 K.

Fig. 8 shows the temperature fields on the four horizontal planes in the stirred tank. Due to the diversion effect of the inner heating coil with a helical structure, the temperature distributions on the four horizontal planes are not uniform. It is clear that Fig 8a located at the level of the coil outlet shows temperature of the region is lowest in the distributions of Fig 8 a, b, c, d. The temperature near the cylinder wall is significantly increased more than the center area of the agitator shaft. Horizontal sections of the top and bottom impellers, Fig 8b and Fig 8c, similarly indicated that near the circular region of the impellers there are ripples of a layer of a minor annular temperature field that gradually increases along the radius direction. It is obvious that the temperature of the cylinder wall layer changed slightly and, with decreasing distance from the cylinder wall the values of temperature declined. The temperature distribution of the horizontal plane of Figure 8d is relatively uniform at the bottom blade position, and the symmetrical trend can be clearly obtained. Therefore, it is a comprehensive conclusion that the improved Intermig impellers provided a preferred mixed heat transfer effect.

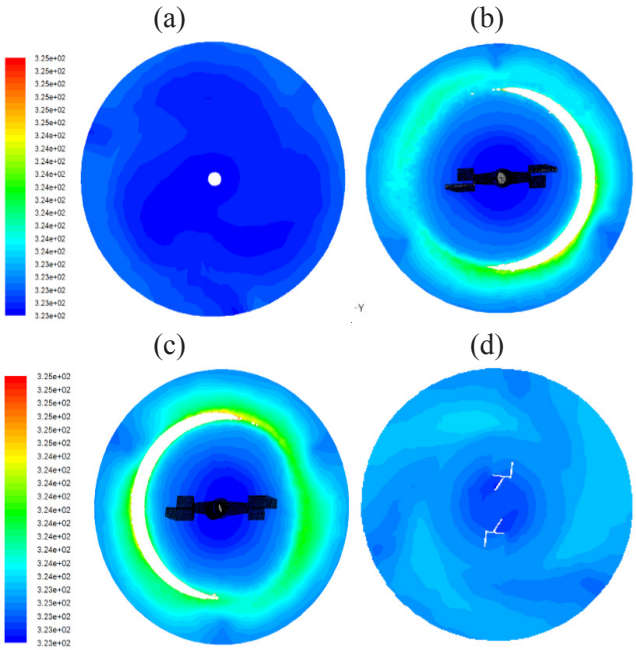

Figure 8. Temperature field distributions on the horizontal sections.

Temperature Boundary Layer

This paper considers the classical problem of thermal boundary layers over the stirred tank with improved Intermig impellers. The five layers of coil outer wall have thermal boundary layers of different thickness, which indicted heat transfer performance of every layer coil. Figure 9 shows the change in

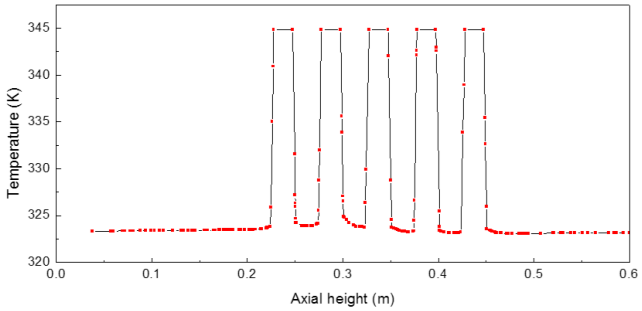

Figure 9. Longitudinal temperature distribution.

temperature in the longitudinal direction at the centre of the inner heating coil (the distance to the centre of the shaft is 0.165 m), for which five temperature peaks appear and the highest temperature is 345 K. Taking the heating coil of the first layer of the bottom location in the stirring vessel as an example, the calibration of the temperature boundary layer is shown in Figure 10. The initial longitudinal height of the calibration starts from 0.220 m, and the curve tends to be stable before 0.224 m, and the temperature is about 323.7 K. The temperature rises sharply from a height of 0.225 m to 0.227 m, and the temperature tends to stabilize at 345 K.

The temperature boundary layer of the coils is divided into five layers from top to bottom, and every layer space can be divided into up-and-down parts. The specific data of the boundary layer thickness are shown in Table 3, and the temperature boundary layers have an average thickness of 3.66 mm, which is much thinner than the temperature boundary layer of the solution (8.9 mm) that was simulated by Delaplace et al. (2001) The lowest thermal boundary layer is located at the down part of layers 1 and 2, corresponding to the positive effect of heat transfer. As the thermal boundary layer decreases, the conclusion that the coil zone far away from impellers possesses a thick thermal boundary layer can be obtained.

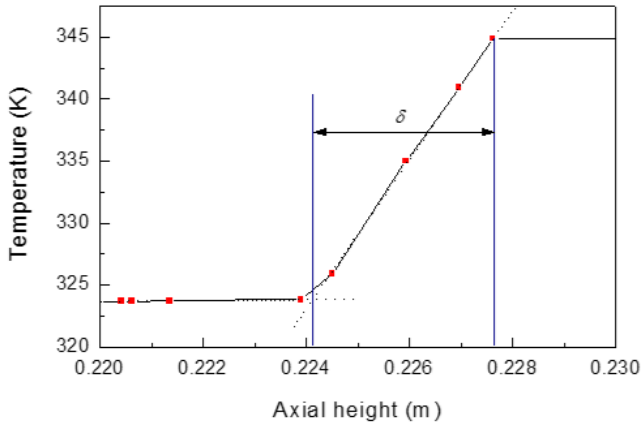

Figure 10. Calibration of the thermal boundary layer thickness.

Table 3. Temperature boundary layer thickness (mm).

Boundary layer location	1	2	3	4	5
Up part	0.0035	0.0033	0.0048	0.0033	0.0042
Down part	0.0032	0.0032	0.0037	0.0039	0.0035

Heat Transfer Coefficient Correlation Outside the Coils

The Reynolds numbers *Re* are between 1.47×10^4 and 1.32×10^5 when the rotational speeds *N* of the improved Intermig impellers are 20, 40, 60, 90, 120, 150 and 180 r/min, and the Reynolds number is listed in Table 4. The convective heat transfer coefficients of the outside coil wall of the simulation and experiment under various speed conditions are also listed in Table 4. The convective heat transfer coefficient of the outside coil wall of the experiment is higher than that of the simulation, and the maximum error for all the Reynolds numbers is 35.13%.

With the increase of the rotating speed, the region around the outside coil reaches a high turbulent state, which is affected by many factors such as the agitator, the inner heating coil and the stirring tank baffles. Thus, the convective heat transfer coefficient of the outside coil changes greatly, and the error of the convective heat transfer coefficient of the outside coil between the simulation and experiment also gradually increases.

The correlation between *Nu* and *Re* in a stirred tank with inner heating coils equipped with dual-layer improved Intermig impellers can be obtained by experiment and simulation. For the internal coil heating stirred tank, the formula of Nagata Eq. (20) is suitable for various traditional mixing paddles (Nagata, 1975). According to the formula of Nagata Eq. (20) and mixing system parameters, the correlation of *Nu* and *Re* in a stirred tank with inner heating coils equipped with dual-layer improved Intermig impellers can be also obtained. The correlations between *Nu* and *Re* obtained by the above three methods are shown in Fig. 11, and the three curves have the same trend and the trends of heat transfer coefficients are consistent and regular.

$$Nu = 2.68\,Re^{0.56}\,Pr^{1/3}\,V_{is}^{-0.14}\left(\frac{d}{D}\right)^{-0.3}\times \times\left(\frac{\sum b_i}{D}\right)^{0.3} N_p^{0.2}\left(\frac{\sum C_i}{iH}\right)^{0.15}(\sin\theta)^{0.5}\left(\frac{H}{D}\right)^{-0.5}\left(\frac{d_{co}}{D}\right) \quad (20)$$

In addition, the correlation between Nu and ε in a stirred tank with inner heating coils equipped with dual-layer improved Intermig impellers can be obtained from the experimental and simulated data in 2.2.1 of this paper. The correlation between *Nu* and ε in a stirred tank with inner heating coils equipped with dual-layer improved Intermig impellers can also be obtained by the fitting formula Eqs. (21) and (22) of Yuji (1982) and mixing system parameters. The correlations between the *Nu* and ε curves obtained by the three methods is shown in Fig. 12, and the three curves are also consistent and regular.

$$Nu = 0.28\left(\frac{\varepsilon d_{co}^4}{\nu^3}\right)^{0.205} Pr^{0.35}\,V_{is}^{-0.14}\left(\frac{d}{D}\right)^{0.2}\times\left(\frac{b}{D}\right)^{0.1}\left(\frac{d_{co}}{D}\right)^{-0.3} \quad (21)$$

$$\left(\frac{\varepsilon d_{co}^{\ 4}}{\nu^3}\right)=\left(\frac{4}{\pi}\right)\left(\frac{d_{co}}{D}\right)^4\left(\frac{D}{d}\right)\left(\frac{D}{H}\right)N_p\,Re^3 \quad (22)$$

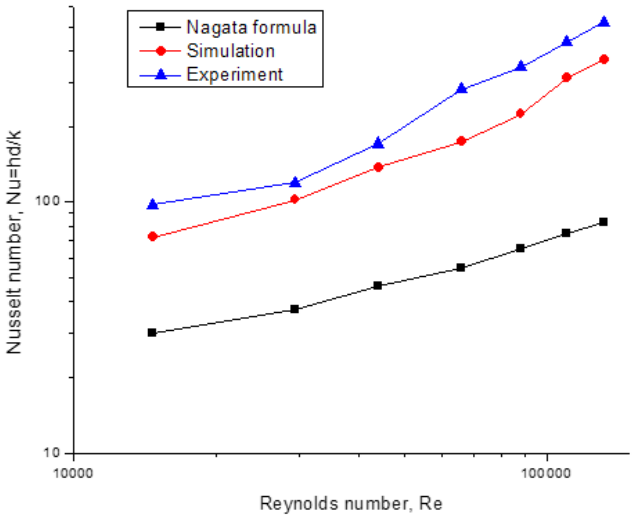

Figure 11. Relationships between *Nu* and *Re*.

It can be seen from Fig. 11 and Fig. 12 that the heat transfer coefficient *Nu* obtained by the simulation

Table 4. Evaluated heat transfer coefficients for different impeller rotation speeds

Rotation speed *N* (rpm)	Reynolds number *Re*	Convective heat transfer coefficient (simulation) h_o(W . m^{-2}K^{-1})	Convective heat transfer coefficient (experiment) h_o(W . m^{-2}K^{-1})	Error
20	14700	2650	3150	15.87%
40	29400	3300	3870	14.75%
60	44100	4440	5530	19.63%
90	66200	5620	7810	28.04%
120	88200	7250	11200	35.13%
150	110000	10100	14100	28.08%
180	132000	12000	16900	29.05%

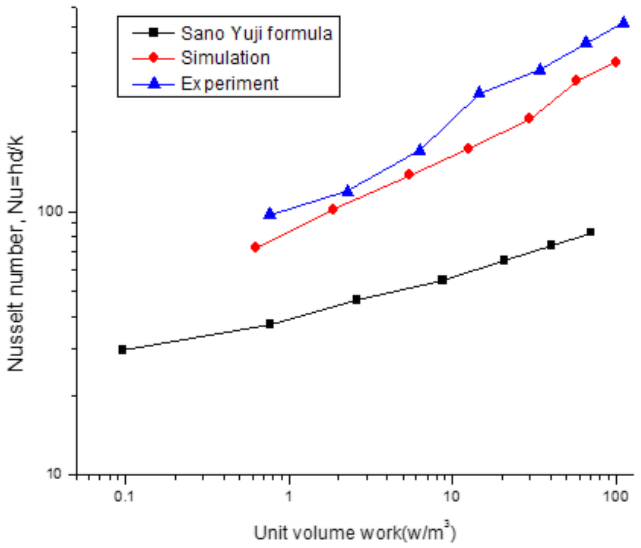

Figure 12. Relationships between Nu and ε.

method is similar to the experimental method, but both of them are much larger than the heat transfer coefficient *Nu* in the curve of the fitting formula from the literature, which indicates that the fitting formula in the literature is too conservative in the calculation of the heat transfer coefficient of the heating coil in the stirred tank with the improved Intermig propeller and that the heat transfer efficiency in stirred tank with dual-layer improved intermig Impellers is higher than that of the traditional blade. Furthermore, the heat transfer coefficients relationship in a stirred tank with inner heating coils equipped with dual-layer improved Intermig impellers is obtained by relevant research data as follows:

$$Nu=0.0337Re^{0.925}Pr^{\frac{1}{3}}\left(\frac{d}{D}\right)^{0.1}\left(\frac{d_{co}}{D}\right)^{0.5} \quad (23)$$

CONCLUSIONS

The heat transfer properties of a dual-layer improved Intermig impeller in a stirred tank with inner heating helical coils were investigated using experiments and simulations. The temperature field, temperature boundary layer of the coil's outer surface and heat transfer coefficient correlations at different rotational speeds were studied. The conclusions are as follows:

(1) Numerical simulations of the temperature field distribution in the tank were performed for different rotational speeds of the Intermig impeller. The errors between the numerical simulations and the experimental measurements are less than 2 K. The temperature inside the tank increases from the top to the bottom and from the inside to the outside; however, the maximum temperature difference is less than 2 K, which indicates the reliability of the simulation method and results.

(2) The temperature boundary layer of the five layers of the coils from top to bottom was calibrated. The average thickness of the temperature boundary layer outside the helical coils is 3.66 mm. When the region around the outside coil reaches a high turbulent state, with the increase of the rotating speed, the error between the simulation and experimental values for the convective heat transfer coefficient of the outside coil in a stirred tank equipped with dual-layer improved Intermig impellers gradually increases.

(3) The heat transfer coefficient correlations including Nu and Re, Nu and ε of the helical coil outer side, were obtained from the simulation and experiment, and the trends of heat transfer coefficients are consistent and regular. Compared with the Nagata method and the Yuji method in the literature, the heat transfer efficiency in stirred tank with the intermig impeller is higher than that of the traditional blade. In addition, the heat transfer coefficient relationship in a stirred tank with inner heating coils equipped with dual-layer improved Intermig impellers is obtained from relevant research data.

ACKNOWLEDGMENTS

This project is supported by the National Natural Science Foundation of China (51775262), the Natural Science Foundation of Jiangsu Province of China (BK20161546) and the Natural Science Foundation for Colleges and Universities in Jiangsu Province of China (16KJA470001)

NOMENCLATURE

A_o	Outside surface area of helical coil, m^2
K_o	Overall heat transfer coefficient, $Wm^{-2}K^{-1}$
D_o	Diameter of the stirred tank, m
d_i	Coil inside diameter, m
d_o	Coil outer diameter, m
S	Pitch, m
F	Heat transfer area, m^2
λ	Thermal conductivity, (W/m.K)
Nu	Nusselt number
Pr	Prandtl number
Q	Overall rate of heat transfer, W
C_p	Specific heat capacity of water at the given temperature, J kg^{-1} K^{-1}
Q_c	Heat flow of Coil of water vapor, W
Q_s	Heat flow of the agitator work, W
Q_h	Heat flow dissipated by air convection, W
ΔE_m	Heat flux absorbed by the bulk material, W
ΔE_w	Heat flow absorbed by the wall of the stirred tank, W
Re	Reynolds number
T_o	Outside temperature of heating water, K
T_i	Inlet temperature of water vapor, K

T_B Average bath temperature of the agitated liquid medium, K
ΔT_{ln} Logarithmic temperature difference between the heating medium and the material, K
k_i Thermal conductivity of water vapor at the given temperature, $Wm^{-1}K^{-1}$
k_o Thermal conductivity of stirring fluid at the given temperature, $Wm^{-1}K^{-1}$
θ Heating time, s
ε Power unit volume
N_p Power number
M Water vapor mass flow, kg/s
x_w Helical coil wall thickness, m
μ Dynamic viscosity of the agitated liquid (heating media) at the mean temperature (Pa S)
μ_w Dynamic viscosity at the inside helical coil (heating media) at the wall temperature (Pa S)

REFERENCES

Broniarz-Press, L., Rozanska, S. Determination of the flow and heat transfer characteristics in non-Newtonian media agitated using the electrochemical technique. International Journal of Heat and Mass Transfer, 51, 910-919 (2008). https://doi.org/10.1016/j.ijheatmasstransfer.2007.11.003

Delaplace, G., Torrez, C., Leuliet, J.-C., Belaubre, N., André, C. Experimental and CFD simulation of heat transfer to highly viscous fluids in an agitated vessel equipped with a non-standard helical ribbon impeller. Chemical Engineering Research and Design, 79, 927-937 (2001). https://doi.org/10.1205/02638760152721460

Delaplace, G., Demeyre, J.F., Guerin, R., Debreyne, P., Leuliet, J.C. Determination of representative and instantaneous process side heat transfer coefficients in agitated vessel using heat flux sensors. Chemical Engineering and Processing: Process Intensification, 44, 993-998 (2005). https://doi.org/10.1016/j.cep.2004.11.005

Delgado, M., Lázaro, A., Mazo, J., Peñalosa, C., Marín, J.M., Zalba, B. Experimental analysis of a coiled stirred tank containing a low cost PCM emulsion as a thermal energy storage system. Energy, 138, 590-601 (2017). https://doi.org/10.1016/j.energy.2017.07.044

Dostál, M., Věříšová, M., Petera, K., Jirout, T., Fořt, I. Analysis of heat transfer in a vessel with helical pipe coil and multistage impeller. The Canadian Journal of Chemical Engineering, 92, 2115-2121 (2014). https://doi.org/10.1002/cjce.22033

Hidalgo-Millán, A., Zenit, R., Palacios, C., Yatomi, R., Horiguchi, H., Tanguy, P.A., Ascanio, G. On the hydrodynamics characterization of the straight Maxblend® impeller with Newtonian fluids. Chemical Engineering Research and Design, 90, 1117-1128 (2012). https://doi.org/10.1016/j.cherd.2012.01.006

Houcine, I., Plasari, E., David, R. Effects of the stirred tank's design on power consumption and mixing time in liquid phase. Chemical Engineering & Technology, 23, 605-613 (2000). https://doi.org/10.1002/1521-4125(200007)23:7%3C605::AID-CEAT605%3E3.0.CO;2-0

Ibrahim, S., Nienow, A.W. Suspension of Microcarriers for Cell Culture with Axial Flow Impellers. Chemical Engineering Research and Design, 82, 1082-1088 (2004). https://doi.org/10.1205/cerd.82.9.1082.44161

Kanamori, H., Yamamoto, T. Characteristics of Heat Transfer Coefficient Distribution at Inside Wall of an Agitated Vessel Based on Data Measured by using a New Measuring Method. Journal of Chemical Engineering of Japan, 44, 908-918 (2011). https://doi.org/10.1252/jcej.11we043

Kougoulos, E., Jones, A.G., Wood-Kaczmar, M. CFD modelling of mixing and heat transfer in batch cooling crystallizers: Aiding the development of a hybrid predictive compartmental model. Chemical Engineering Research and Design, 83, 30-39 (2005). https://doi.org/10.1205/cherd.04080

Liu., B., Zhang, Y., Liu, J., Qian, L., Li, P., Jin, Z. Research on heat transfer performance of coaxial mixer with inner combined impeller. Industrial & Engineering Chemistry Research, 52, 17285-17293 (2013). https://doi.org/10.1021/ie401499f

Nagata S. Mixing: principles and applications. Halsted Press (1975).

Perarasu, V.T., Arivazhagan, M., Sivashanmugam, P. Heat transfer of TiO_2/water nanofluid in a coiled agitated vessel with propeller. Journal of Hydrodynamics, 24, 942-950 (2012). https://doi.org/10.1016/S1001-6058(11)60322-3

Perarasu, T., Arivazhagan, M., Sivashanmugam, P. Experimental and CFD heat transfer studies of Al_2O_3-water nanofluid in a coiled agitated vessel equipped with propeller. Chinese Journal of Chemical Engineering, 21, 1232-1243 (2013).

Prada, R.J., Nunhez, J.R. Numerical prediction of a nusselt number equation for stirred tanks with helical coils. AIChE Journal, 63, 3912-3924 (2017). https://doi.org/10.1002/aic.15765

Szalai, E.S., Arratia, P., Johnson, K., Muzzio, F.J. Mixing analysis in a tank stirred with Ekato Intermig® impellers. Chemical Engineering Science, 59, 3793-3805 (2004). https://doi.org/10.1016/j.ces.2003.12.033

Triveni, B.,Vishwanadham, B., Venkateshwar, S. Studies on heat transfer to Newtonian and non-Newtonian fluids in agitated vessel. International Journal of Heat and Mass Transfer, 44, 1281-1288 (2008). https://doi.org/10.1007/s00231-007-0364-2

Wang, C., Xu, Y., Wu, Y., An, Z. PIV investigation of the flow features of double and single 45° up□ pumping pitched blade turbines in a square tank. The Canadian Journal of Chemical Engineering, 96, 788-799 (2018). https://doi.org/10.1002/cjce.22952

Xie, M.-H., Xia, J.-Y., Zhou, Z., Zhou, G.-Z., Chu, J., Zhuang, Y.-P., Zhang, S.-L., Noorman. H. Power consumption, local and average volumetric mass transfer coefficient in multiple-impeller stirred bioreactors for xanthan gum solutions. Chemical Engineering Science, 106, 144-156 (2014). https://doi.org/10.1016/j.ces.2013.10.032

Yuji, S., Hiro, I., Eiji, N. Correlation of power and heat transfer coefficient outside the heat exchanger of inner-heating coils in a stirred tank. Chemical Engineering (China), 60-65 (1982).

Zakrzewska, B., Jaworski, Z. CFD modeling of turbulent jacket heat transfer in a Rushton turbine stirred vessel. Chemical Engineering & Technology, 27, 237-242 (2004). https://doi.org/10.1002/ceat.200401988

Zhao, H.L., Zhang, Z.M., Zhang, T.A., Yan, L.I.U., Gu, S.Q., Zhang, C. Experimental and CFD studies of solid-liquid slurry tank stirred with an improved Intermig impeller. Transactions of Nonferrous Metals Society of China, 24, 2650-2659 (2014). https://doi.org/10.1016/S1003-6326(14)63395-1

Zhao, H.L., Lv, C., Liu, Y., Zhang, T.A. Process optimization of seed precipitation tank with multiple impellers using computational fluid dynamics. JOM, 67, 1451-1458 (2015). https://doi.org/10.1007/s11837-015-1401-0